DOI: 10.1002/adma.200502711

Intrinsic Ferroelectric Properties of Strained Tetragonal $PbZr_{0.2}Ti_{0.8}O_3$ Obtained on Layer–by–Layer Grown, Defect–Free Single–Crystalline Films**

By *Ionela Vrejoiu*,* *Gwenaël Le Rhun*, *Lucian Pintilie*, *Dietrich Hesse*, *Marin Alexe*, and *Ulrich Gösele*

In many materials of technological interest, especially in semiconductors, structural defects play detrimental roles.[1,2] In the case of silicon (and other semiconductors) defects have to be thoroughly controlled. The growth of defect–free single crystals is a prerequisite for the accurate assessment of intrinsic physical properties of silicon, such as electronic band structure, optical bandgap, carrier densities, and so forth. If large single crystals cannot be grown, as in the case of the ferroelectric $PbZr_{0.2}Ti_{0.8}O_3$ perovskite, intrinsic properties can be studied on single–crystalline films, if the quality of growth permits the achievement of films that are free from extended defects.

Here, we report on the intrinsic physical properties of strained, defect–free, single–crystalline $PbZr_{0.2}Ti_{0.8}O_3$ films synthesized by pulsed laser deposition (PLD). $PbZr_xTi_{1-x}O_3$ (PZT) ferroelectrics are considered for most applications involving ferroelectric oxide materials, from piezoelectric transducers to dynamic nonvolatile random access memories. The incongruent melting of $PbZrO_3$ and $PbTiO_3$ as well as the high volatility of PbO at growth temperatures pose a challenge in establishing the equilibrium of bulk crystals of PZT.[3] Therefore, single–domain single crystals of PZT have never been synthesized for a significant compositional range across the solid–solution phase. This leaves the intrinsic properties of single–domain PZT crystals under debate.[4] Hence, the growth of single–crystalline defect–free PZT thin films may enable the study of fundamental physical properties. For instance, the spontaneous polarization P_S, which is a fundamental parameter that defines the performance of a ferroelectric material, is rarely reported due to the lack of single crystals[4] and perfectly polar–axis–oriented films.[5,6] Although the macroscopic polarization is the basic quantity used to describe ferroelectrics, it has long escaped precise microscopic definition. It has been pointed out that previously calculated values[4] of the polarization may thus be incorrect, due to invalid definitions and models employed for their computation.[7] Novel concepts such as polarization as a Berry phase of the electronic Bloch wavefunctions have been recently introduced.[8,9]

Additionally, accurate investigations of the highly debated issue of size effects in nanostructured ferroelectrics demand the growth of materials free from extended defects, to rule out the extrinsic contribution of defects to the disappearance/suppression of ferroelectricity below a certain critical size.[10,11]

The fabrication of defect–free single–crystalline ferroelectric thin films requires careful choice of a single–crystalline substrate and its crystallographic surface termination, a suitable growth technique, and–most importantly–appropriate growth parameters. It is necessary to employ a single–crystalline substrate with closely matched lattice constants. In mismatched epitaxial films which grow in a two–dimensional mode (i.e., step–flow or layer–by–layer growth) biaxial stress is generated. Usually, the stress relaxation in mismatched epitaxial films leads to the formation of misfit dislocations (MDs) at the film/substrate interface,[12–14] which are commonly accompanied by threading dislocations (TDs) that extend across the film.[12] It has been demonstrated that MDs have an important impact on the ferroelectric properties of nanostructured ferroelectric perovskites.[15,16]

PLD is suitable for synthesis of high–quality homo– and heteroepitaxial films. This is due to the highly supersaturated ablation plasma plume, its pulsed nature, and the adjustable deposition rate attainable by changing the laser energy density, laser repetition rate, background reactive gas pressure, and target–to–substrate distance (d_{TS}).[17–19]

Bearing in mind the aforementioned reasoning, we chose to grow epitaxial PZT films onto well–defined vicinal $SrTiO_3$(001) (STO) substrates of uniform surface termination by using PLD. First $SrRuO_3$ (SRO) was deposited on STO as the bottom electrode, also by using PLD. SRO is an excellent template for the heteroepitaxial growth of high–quality ferroelectric perovskites, as it grows in a single–crystalline manner and can be grown as an atomically flat surface on vicinal STO(001) substrates.[20] Concerning PZT, we focused on the $PbZr_{0.2}Ti_{0.8}O_3$ composition, since it has a *bulk* in–plane lattice parameter of 3.935 Å, which is closely matched to that of SRO (3.928 Å), and has a rather small misfit to the slightly smaller lattice parameter of the cubic STO substrate (3.905 Å). Nevertheless, under such circumstances, it is ex-

[*] Dr. I. Vrejoiu, Dr. G. Le Rhun, Dr. L. Pintilie, Dr. D. Hesse, Dr. M. Alexe, Prof. U. Gösele
Max Planck Institute of Microstructure Physics
Weinberg 2, 06120 Halle (Germany)
E-mail: vrejoiu@mpi–halle.de

[**] The work has been partly funded by Volkswagen Foundation, through the "Nanosized ferroelectric hybrids" project no. I/80897. Sincere thanks to S. Reyntjens and E. Sourty, both from FEI Application Laboratory (Eindhoven/NL), for the FIB preparation and STEM investigation, respectively, to N. D. Zakharov for HRTEM investigations, to S. Swatek for the TEM sample preparation, and N. Schammelt for assistance in the PLD system maintenance.

ADVANCED MATERIALS

pected that compressive biaxial strain builds up in the heteroepitaxially grown SRO and PZT layers, which may enhance the tetragonality of the $PbZr_{0.2}Ti_{0.8}O_3$ thin films.

Detailed microstructural investigations, macroscopic measurements of room–temperature ferroelectric polarization and dielectric constant, and local measurements of the piezoelectric coefficient were performed to characterize the single–crystalline PZT films.

The surface morphology of the layers was investigated by atomic force microscopy (AFM). The SRO layer grew atomically flat, with one–unit–cell stepped terraces (step–flow growth regime) (Fig. 1b), following the terraces of the vicinal STO substrate (Fig. 1a).[20] It was previously pointed out that the flatness of STO and SRO surfaces plays an important role in the growth of ultrathin PZT films.[21] AFM images taken on the surface of an ultrathin PZT film (film thickness, $t \approx 3$ nm) reveal that, at the initial stage of the growth, the PZT layer grows by filling the terraces of the template SRO layer (Fig. 1c), and layer–by–layer growth[22] prevails also for much thicker PZT layers ($t \approx 90$ nm), as shown in Figure 1d. When the layer–by–layer growth regime is achieved, the indications are that epitaxy results in almost all circumstances provided that the substrate surface is clean enough and well prepared. In this regime the substrate has a very strong influence on the form of the film produced, and the growing film has little option but to choose the best (i.e., necessarily epitaxial) orientation in which to grow.[22] In our case the quality of the STO crystals employed as substrates has been rather critical. Adequate preparation of the STO vicinal substrates prior to their use for PLD (see Experimental section for details, along with details about the PLD synthesis of the SRO and PZT films) has proven to be an important step in the fabrication of defect–free heteroepitaxial thin films.

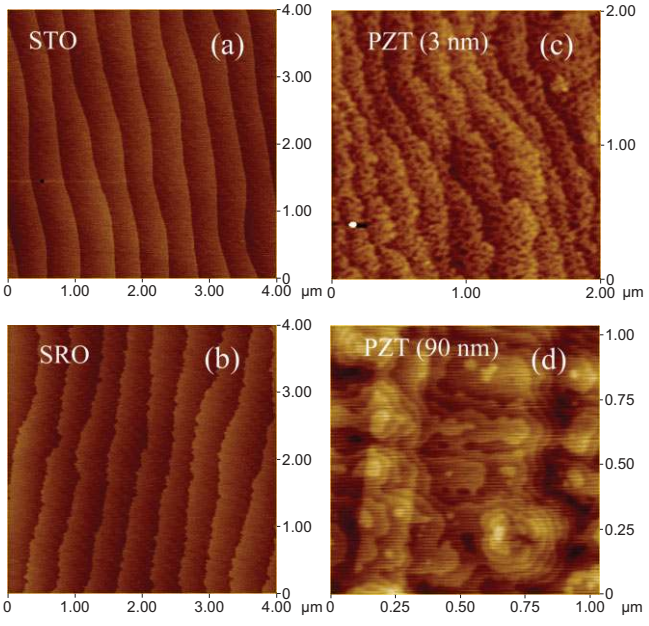

Figure 1. AFM images of the vicinal STO substrate and the epitaxially PLD–grown SRO and $PbZr_{0.2}Ti_{0.8}O_3$ layers. The one–unit–cell stepped terraces (400 nm wide) of an STO substrate are visible in (a). The morphology of the SRO, step–flow grown (film thickness, $t = 20$ nm) on this substrate, is shown in (b). In (c) and (d) the morphology of layer–by–layer grown ultrathin ($t \approx 3$ nm) and thick ($t \approx 90$ nm) $PbZr_{0.2}Ti_{0.8}O_3$ films deposited on top of SRO/STO heterostructures are displayed.

Cross–sectional transmission electron microscopy (TEM), atomic number (Z)–contrast scanning transmission electron microscopy (STEM), and electron diffraction investigations revealed the entire heterostructure to be epitaxial, and the interfaces between the layers to be plane and atomically sharp (Fig. 2a,c, and d). TEM allowed the measurement of the layer thicknesses, that is, 20 nm for the SRO layer and 90—100 nm for the PZT layer (Fig. 2a). 90° domains, which are typical for tetragonal perovskite ferroelectric films, were not formed in the PZT layer. This confirms that the PZT layer is strained and the strain was not relieved by the formation of twins.[23,24] Polydomain formation in epitaxial films undergoing a phase transformation is a mechanism that relaxes the total strain energy, which is the result of lattice misfit, the difference in the thermal expansion coefficients of the film and the substrate, and misfit dislocation formation.

High–resolution TEM (HRTEM) of an ultrathin PZT film (8—9 nm) grown also in the layer–by–layer mode reveals that the PZT layer is perfectly strained to match the SRO lattice parameter (Fig. 2c). No misfit dislocations were formed in the PZT layer. High–resolution STEM Z–contrast microscopic images of a 30 nm thick PZT film confirmed this very good matching and the absence of misfit dislocations, as shown in Figure 2d. Hence, we were able to grow films that are free from any *extended* structural defects, with film thicknesses from a few to several hundreds of nanometers. The possible existence of point defects, such as oxygen vacancies, cannot be accounted for from TEM investigations. For thin films with such a complex stoichiometry as PZT, it is extremely difficult to accurately assess their precise oxygen content. However, we are confident that our thin films have no significant oxygen deficiency, as indicated by their remarkably good ferroelectric properties.

For comparison, we show also the TEM cross–sectional image of an epitaxial PZT film of about the same thickness that has structural defects. This layer was synthesized with the same PLD parameters using a $Pb_{1.1}(Zr_{0.2}Ti_{0.8})O_3$ target that we suspect to be slightly oxygen deficient (Fig. 2e). This PZT layer has a considerably more defective microstructure and exhibits 90° domains. At the SRO/PZT interface, a defective thin layer formed, which was evidenced by HRTEM as well (not shown here).

From the electron diffraction pattern shown in Figure 2b, the tetragonality ratio of the defect–free PZT layer could be calculated, $c/a \approx 1.06$. This is considerably higher than that of bulk PZT with this composition, which has a room–temperature value of $c/a = 1.051$.[25] Recently, Morioka et al.[5] reported on similar investigations made on epitaxial PZT films with various compositions; however, they did not focus on the PZT composition we report on. The authors studied the orientation of their ferroelectric films by means of high–resolution X–ray

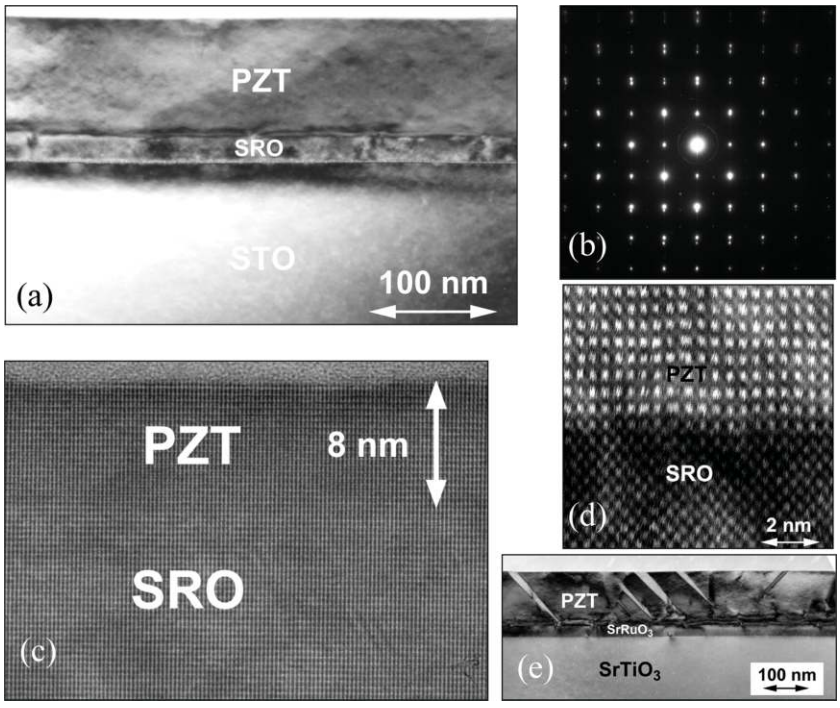

Figure 2. TEM investigations of the $PbZr_{0.2}Ti_{0.8}O_3$/SRO/STO heterostructures. The images are: a) cross–sectional TEM image of a defect–free PZT film (t = 90 nm) on top of an SRO film (t = 20 nm) grown on vicinal STO (001), b) electron diffraction pattern of this heterostructure, c) high–resolution TEM (HRTEM) image of an ultrathin PZT film (t = 8 nm), d) Z–contrast STEM image showing the sharp and dislocation–free interface between the PZT and SRO layers of such a heterostructure, and e) cross–sectional TEM image of a defective PZT film (t = 120 nm) on top of an SRO film (t = 20 nm) grown on vicinal STO (001).

diffraction (XRD), being thus able to measure only the volume fraction of 90° domains present in their tetragonal PZT films. TEM was not employed in their work. However, XRD was unable to ascertain the possible existence of extended structural defects, such as dislocations, in heteroepitaxial films. TEM investigations are therefore mandatory when proof of the perfection of the crystalline structure is required. Morioka et al.[5] also showed the relationship between P_S and $c/a-1$ for tetragonal PZT. From the corresponding curve (shown in Fig. 5 of their paper), a value of $P_S \approx 110\ \mu C\,cm^{-2}$ would result for $c/a \approx 1.058$.

The ferroelectric and piezoelectric properties of our PZT films were investigated in detail. Ferroelectric polarization and switching–current hysteresis curves are shown in Figure 3a. The measurements were performed on the defect–free PZT film (90 nm thick) shown in Figure 2a. The polarization hysteresis curve has a square shape, remnant polarization being as high as $P_r \approx 105 \pm 5\ \mu C\,cm^{-2}$, and basically equal to the P_S. The polarization showed only a weak frequency dependence (within 10 %). This value is, to the best of our knowledge,

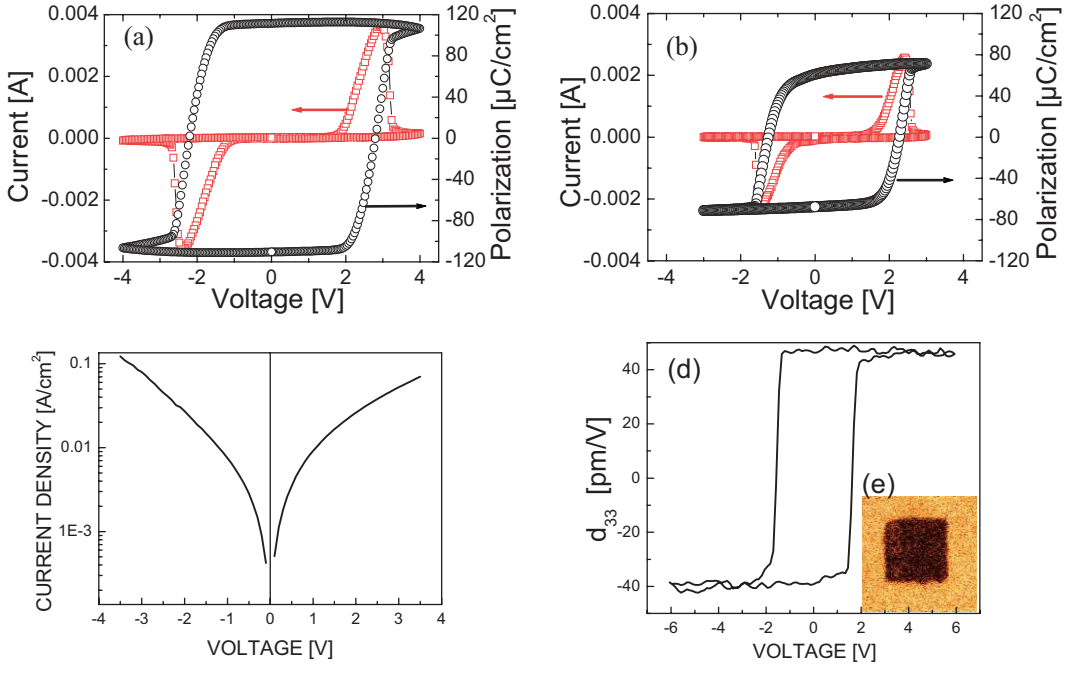

Figure 3. Ferroelectric and piezoelectric investigations of the $PbZr_{0.2}Ti_{0.8}O_3/SrRuO_3/SrTiO_3$ heterostructures. Ferroelectric hysteresis curves measured at 1 kHz are shown for a) a defect–free PZT film (remnant polarization, P_r = 105 <M+–> 5 $\mu C\,cm^{-2}$) and b) a defective film (P_r = 65 $\mu C\,cm^{-2}$). Leakage current density versus voltage measured on the defect–free PZT layer is shown in (c) and local piezoelectric coefficient (d_{33}) hysteresis of the same layer is displayed in (d). The inset (e) is a 1 μm × 1 μm piezoresponse image, where the center area (0.5 μm × 0.5 μm) has switched polarization by being scanned with the tip under DC bias. No backswitching was observed after a time as long as 71 h.

ADVANCED MATERIALS

the highest value reported for PZT epitaxial films with the considered composition.[5,11,26–28] It exceeds also the value of the remnant polarization recently reported for single *c*–domain heteroepitaxial $PbTiO_3$ films.[29] It is also higher than the theoretical value, $P_r = 70\ \mu C\,cm^{-2}$, calculated for bulk single crystals.[4] It is, nevertheless, in very good agreement with the value of the tetragonality ratio mentioned above and the relationship given in Figure 5 of the paper of Morioka et al.[5] We mention here that recent calculations[30] for $PbTiO_3$ that undergoes anomalous enhancement of tetragonality predict values of the spontaneous polarization as high as $P_S \approx 140\ \mu C\,cm^{-2}$.

The hysteresis loop measured under the same conditions on the PZT layer with structural defects shown in Figure 2e is displayed in Figure 3b for comparison. The shape is less square and the remnant polarization much lower, $P_r \approx 65\ \mu C\,cm^{-2}$. This should be a consequence of the 90° domains and the more defective microstructure of this epitaxial PZT layer.

Figure 3c displays the leakage current density for the defect–free layer. The slight asymmetry of the two branches of the curve indicates that interface–controlled injection of carriers occurs. Even though both the bottom and the top electrodes consisted of SRO, they were deposited under different conditions, and therefore the interfaces may have different properties, namely different interface state densities and potential barrier heights. The leakage current density has a rather large value, especially when compared with the leakage currents measured in polycrystalline PZT films.[31] We suppose that in defect–free single–crystalline films the carrier mobility is much higher than in a defective film. Polycrystalline films exhibit extended defects (i.e., grain boundaries, domains) that may scatter the injected carriers, thus reducing their mobility, and may trap the carriers, thus decreasing their density. Nevertheless, we should mention that the relatively high leakage current density of our defect–free single–crystalline PZT films does not hinder in any way the ferroelectric switching.

The dielectric constant was estimated from capacitance measurements. The obtained value was around $\varepsilon_{33} = 90 \pm 5$, which is significantly lower than the values reported by other groups for *c*–axis oriented epitaxial PZT films.[6,28,32] However, it is in good agreement with a theoretical value that Haun et al.[4] estimated for bulk single crystals of PZT with this composition. For the defective layer that has 90° domains (Fig. 2e), based on capacitance measurements, we estimated the effective dielectric permittivity to be about 170. This is an indication that the value we measured for the defect–free PZT layer, $\varepsilon_{33} = 90 \pm 5$, is the intrinsic value of dielectric permittivity, as there are no extended defects, such as 90° domains and grain boundaries, that may extrinsically enhance the measured dielectric permittivity.[33–36] Phase–field simulations performed by Li et al.[34] for tetragonal epitaxial $PbZr_{0.2}Ti_{0.8}O_3$ films subjected to *tensile* biaxial strain indicated that the out–of–plane dielectric constant ε_{33} has a larger value in a film with a large volume fraction of 90° domains. No simulation results were shown by the aforementioned authors for the case of tetragonal epitaxial PZT films under *compressive* biaxial strain.

Local piezoresponse behavior was investigated by scanning probe microscopy. The investigations revealed that the PZT layer has an out–of–plane polarization that is preferentially oriented in the as–grown state[37,38] and confirmed the absence of 90° domains, as can be seen in the inset of Figure 3d. The piezoresponse hysteresis curve plotted in Figure 3d has a square shape and the value of the d_{33} piezoelectric coefficient was estimated to be around $d_{33} = 45 \pm 5\ pm\,V^{-1}$,[4,38] that is also a theoretical value for $PbZr_{0.2}Ti_{0.8}O_3$ single–domain strained films on $SrTiO_3$.[27] The inset in Figure 3d shows the piezoresponse measured 71 h after poling the center of the scanned region (1 μm × 1 μm) with negative bias (–5 V) to switch the polarization direction. No backswitching of the reversed polarization to the as–grown polarization state occurred.

In conclusion, we have synthesized and studied defect–free single–crystalline $PbZr_{0.2}Ti_{0.8}O_3$ thin films on SRO–coated STO (001) vicinal single crystals. The PZT films have square–shape polarization and piezoelectric hysteresis loops, remnant polarization values of up to $P_r = 105 \pm 5\ \mu C\,cm^{-2}$, a dielectric constant $\varepsilon_{33} = 90 \pm 5$, and a piezoelectric coefficient of up to $d_{33} = 45 \pm 5\ pm\,V^{-1}$. Both macroscopic ferroelectric measurements and local piezoresponse investigations point out a remarkable ease of polarization switching, which is likely to be the consequence of the lack of defects in the PZT layer. Synthesis of defect–free single crystalline films enabled us to unambiguously determine fundamental intrinsic quantities that describe ferroelectric materials, such as spontaneous polarization and dielectric constant, and will allow a more reliable study of size effects in defect–free nanostructured ferroelectrics.

Experimental

Vicinal single–crystalline STO(001) substrates with a miscut angle of 0.05°—0.2° (CrysTec, Berlin) were used to epitaxially grow the heterostructure. The STO substrates were etched in a buffered HF solution and annealed in air at temperatures between 950 and 1100 °C, depending on the miscut angle [19,20]. Thus, after adequate selection and preparation, one–unit–cell stepped terraces with straight ledges formed. The layers were fabricated by PLD, employing a KrF excimer laser (wavelength, $\lambda = 248$ nm). Ceramic $SrRuO_3$ and $Pb_{1.1}(Zr_{0.2}Ti_{0.8})O_3$ targets (PRAXAIR) were used for PLD. The SRO layer ($t = 20—100$ nm) was deposited at a substrate temperature, $T = 700$ °C in a background atmosphere of 100 mTorr (1 mTorr ≈ 0.133 Pa) oxygen, with a laser fluence (energy density), $\Phi_L = 1.5—2\ J\,cm^{-2}$, at a laser repetition rate, $\nu_L = 5$ Hz, and $d_{TS} \approx 5.5$ cm. The subsequent PZT layer ($t = 2—275$ nm) was grown at $T = 575$ °C in 200 mTorr oxygen, $\Phi_L = 2—3\ J\,cm^{-2}$, and at $\nu_L = 3$ or 5 Hz. The deposition rate is a critical parameter both for the step–flow growth of single–crystalline strained SRO on vicinal STO substrates [20] and for the subsequent layer–by–layer growth of defect–free, strained PZT thin films. For PLD, control over the deposition rate was achievable by careful optimization of the laser fluence, laser repetition rate, d_{TS}, and oxygen pressure. For a fixed d_{TS}, a certain deposition temperature (between 600 and 700 °C for SRO, and not much higher than 600 °C for PZT) and oxygen pressure, one has to adjust

the laser fluence and repetition rate according to the terrace width of the employed vicinal STO substrate, as already pointed out by Hong et al. [20].

Circular SRO top electrodes (pads of 340 μm diameter) were deposited by PLD at room temperature through a shadow mask and then platinum was deposited by sputtering on top of the SRO, in order to ease the contacting of the capacitor pads.

TEM samples were prepared by standard mechanical and ion–beam thinning procedures [39]. The cross–sectional sample used for *Z*–contrast STEM investigations of the interfaces was prepared by a focused–ion–beam technique. TEM was performed in a Philips CM20T microscope, and STEM in an FEI Tecnai G^2F20 Xtwin microscope, both operated at 200 kV.

Macroscopic ferroelectric hysteresis, fatigue, and leakage current curves were acquired [40] using the TF2000 Analyzer (AixaCCT). The capacitance measurements were performed at zero DC voltage and with an amplitude of 50 mV for the 1 kHz AC probe signal.

Local piezoresponse behavior was investigated using a scanning probe microscope (ThermoMicroscopes). PtIr–coated tips (Nanosensors, ATEC–EFM) with an elastic constant of about 2.5 $N\,m^{-1}$ were employed. A local piezoelectric hysteresis curve was acquired by superimposing a DC bias voltage to the AC probing voltage (1 V, 22.3 kHz). For quantitative measurements the piezoresponse signal was previously calibrated using an *x*–cut quartz ($d_{33} = 2.17$ pm V^{-1}).

Received: December 20, 2005
Final version: March 9, 2006
Published online: June 8, 2006

[1] S. K. Estreicher, *Mater. Today* **2003**, *6*, 26.
[2] H. J. Queisser, E. E. Haller, *Science* **1998**, *281*, 945.
[3] S. Aggarwal, R. Ramesh, *Annu. Rev. Mater. Sci.* **1998**, *28*, 463.
[4] M. J. Haun, E. Furman, S. J. Jang, L. E. Cross, *Ferroelectrics* **1989**, *99*, 63.
[5] H. S. Morioka, S. Yokoyama, T. Oikawa, H. Funakubo, K. Saito, *Appl. Phys. Lett.* **2004**, *85*, 3516.
[6] Y. K. Kim, H. Morioka, R. Ueno, S. Yokoyama, H. Funakubo, *Appl. Phys. Lett.* **2005**, *86*, 212 905.
[7] D. Vanderbilt, R. D. King–Smith, *Phys. Rev. B* **1993**, *48*, 4442.
[8] R. Resta, *Europhys. News* **1997**, *28*, 18.
[9] N. Sai, K. M. Rabe, D. Vanderbilt, *Phys. Rev. B* **2002**, *66*, 104 108.
[10] J. Junquera, P. Ghosez, *Nature* **2003**, *422*, 506.
[11] V. Nagarajan, S. Prasertchoung, T. Zhao, H. Zheng, J. Ouyang, R. Ramesh, W. Tian, X. Q. Pan, D. M. Kim, C. B. Eom, H. Kohlstedt, R. Waser, *Appl. Phys. Lett.* **2004**, *84*, 5225.
[12] E. A. Fitzgerald, *Mater. Sci. Rep.* **1991**, *7*, 87.
[13] A. Y. Emelyanov, N. A. Pertsev, *Phys. Rev. B* **2003**, *68*, 214 103.
[14] S. Y. Hu, Y. L. Li, L. Q. Chen, *J. Appl. Phys.* **2003**, *94*, 2542.
[15] M.–W. Chu, I. Szafraniak, R. Scholz, C. Harnagea, D. Hesse, M. Alexe, U. Gösele, *Nat. Mater.* **2004**, *3*, 87.
[16] V. Nagarajan, C. J. Lia, H. Kohlstedt, R. Waser, I. B. Misirlioglu, S. P. Alpay, R. Ramesh, *Appl. Phys. Lett.* **2005**, *86*, 192 910.
[17] D. Bäuerle, *Laser Processing and Chemistry*, 3rd ed., Springer, New York **2000**.
[18] P. R. Willmott, J. R. Huber, *Rev. Mod. Phys.* **2000**, *72*, 315.
[19] G. Koster, *Ph.D. Thesis*, University of Twente, The Netherlands **1999**.
[20] W. Hong, H. N. Lee, M. Yoon, H. M. Christen, D. H. Lowndes, Z. Suo, Z. Zhang, *Phys. Rev. Lett.* **2005**, *95*, 095 501.
[21] H. Nonomura, H. Fujisawa, M. Shimizu, H. Niu, *Jpn. J. Appl. Phys., Part 1* **2002**, *41*, 6682.
[22] J. W. Matthews, *Epitaxial Growth Part B*, Academic, New York **1975**, Ch. 4.
[23] A. L. Roitburd, *Phys. Status Solidi A* **1976**, *37*, 329.
[24] V. Nagarajan, I. G. Jenkins, S. P. Alpay, H. Li, S. Aggarwal, L. Salmanca–Riba, A. L. Roytburd, R. Ramesh, *J. Appl. Phys.* **1999**, *86*, 595.
[25] Y. Li, V. Nagarajan, S. Aggarwal, R. Ramesh, L. G. Salamanca–Riba, L. J. Martinez–Miranda, *J. Appl. Phys.* **2002**, *92*, 6762.
[26] V. Nagarajan, A. Roytburd, A. Stanishevsky, S. Prasertchoung, T. Zhao, L. Chen, J. Melngailis, O. Auciello, R. Ramesh, *Nat. Mater.* **2002**, *2*, 43.
[27] N. A. Pertsev, V. G. Kukhar, H. Kohlstedt, R. Waser, *Phys. Rev. B* **2003**, *67*, 054 107.
[28] C. M. Foster, G.–R. Bai, R. Csencsits, J. Vetrone, R. Jammy, L. A. Willis, E. Carr, J. Amano, *J. Appl. Phys.* **1997**, *81*, 2349.
[29] W. W. Jung, H. C. Lee, W. S. Ahn, S. H. Ahn, S. K. Choi, *Appl. Phys. Lett.* **2005**, *86*, 252 901.
[30] S. Tinte, K. M. Rabe, D. Vanderbilt, *Phys. Rev. B* **2003**, *68*, 144 105.
[31] L. Pintilie, I. Boerasu, M. J. M. Gomes, T. Zhao, R. Ramesh, M. Alexe, *J. Appl. Phys.* **2005**, *98*, 124 104.
[32] S. Yokoyama, Y. Honda, H. Morioka, S. Okamoto, H. Funakubo, T. Iijima, H. Matsuda, K. Saito, T. Yamamoto, H. Okino, O. Sakata, S. Kimura, *J. Appl. Phys.* **2005**, *98*, 094 106.
[33] F. Xu, S. Trolier–McKinstry, W. Ren, B. Xu, X.–L. Xie, J. Hemker, *J. Appl. Phys.* **2001**, *89*, 1336.
[34] Y. L. Li, S. Y. Hu, L. Q. Chen, *J. Appl. Phys.* **2005**, *97*, 034 112.
[35] C. Ang, Z. Yu, *Appl. Phys. Lett.* **2004**, *85*, 3821.
[36] C. Ang, Z. Yu, *Phys. Rev. B* **2004**, *69*, 174 109.
[37] C. S. Ganpule, V. Nagarajan, H. Li, A. S. Ogale, D. E. Steinhauer, S. Aggarwal, E. Williams, R. Ramesh, P. De Wolf, *Appl. Phys. Lett.* **2000**, *77*, 292.
[38] G. Le Rhun, I. Vrejoiu, L. Pintilie, D. Hesse, M. Alexe, U. Gösele, *Nanotechnology* **2006**, in press.
[39] D. B. Williams, C. B. Carter, *Transmission Electron Microscopy*, Plenum, New York **1996**.
[40] L. Pintilie, I. Vrejoiu, D. Hesse, M. Alexe, *Appl. Phys. Lett.* **2006**, *88*, 102 908.

